Ancora, D., Valentini, G., Pifferi, A. G., & Bassi, A. (2021, March). Auto-correlation for multi-view deconvolved reconstruction in light sheet microscopy. In Three-Dimensional and Multidimensional Microscopy: Image Acquisition and Processing XXVIII (Vol. 11649, p. 116490X). International Society for Optics and Photonics.

https://doi.org/10.1117/12.2583004

Auto-correlation for multi-view deconvolved reconstruction in light sheet microscopy

Daniele Ancora[1,*], Gianluca Valentini[1,2], Antonio Pifferi[1,2], and Andrea Bassi[1,2]

[1]Dipartimento di Fisica, Politecnico di Milano, Piazza Leonardo da Vinci 32, 20133 Milano, Italy
[2]Istituto di Fotonica e Nanotecnologie, Consiglio Nazionale delle ricerche, Piazza Leonardo da Vinci 32, 20133 Milano, Italy

ABSTRACT

Tomographic inspection of fluorescent labels distributed within a specimen is an important aspect in biology. Light sheet fluorescent microscopy (LSFM) offers a powerful and simple tool to selectively slice the sample and let us directly obtain a tomographic view of the specimen. However, due to non-isotropic resolution of the technique along the axial scanning, one may want to combine different views of the object and add deconvolution to the process in order to achieve higher resolution. Typically, multi-view Bayesian methods based on Richardson-Lucy deconvolution are used for this task once the datasets are exactly registered against each other. In this work, instead, we begin to investigate how to avoid the alignment procedure and use a direct algorithm to form a multi-view tomographic reconstruction. To do this, we developed a new framework based on auto-correlation analysis that let us achieve deconvolved reconstructions starting from blurred auto-correlations. Since the latter are insensitive to shifts, we can combine the auto-correlations coming from multi-view acquisitions without taking care of the registration procedure.

Keywords: Auto-correlation imaging, phase retrieval, computed tomography, biomedical imaging, inverse problems.

1. INTRODUCTION

The light-sheet fluorescent microscopy[1] (LSFM) is a well established technique for inspecting internal feature of a three-dimensional specimen. The idea behind LSFM is to slice the sample by forming a light sheet orthogonal to the detection axis. In this way, it is possible to excite only the fluorescence in that region, that can be recorded excluding all the remaining volume. By translating the sample through the light-sheet and acquiring each time the camera image, it is possible to form a tomographic-stack that contains the spatial distribution of the fluorescence emitted by the specimen. In its simplistic implementation, there is no strict need for any computational processing of the dataset acquired. However, there are situations in which a multi-view of the specimen is required to achieve better imaging resolution,[2,3] in particular when trying to image specimens larger than a transport-mean-free-path.[4] In this case, the acquisitions done orienting the object at different angles help to reconstruct features located on the opposite side (with respect the view point) or hidden by the sample. It is crucial to perfectly align the views before their fusion. Normally, we accomplish this by evaluating cross-correlation displacement between the views oriented to the same angular observation. Instead, auto-correlations offer a radically different approach to the problem. They have been already used to enable alignment-free optical projection tomography[5] and for hidden three-dimensional reconstructions.[6] In both cases, we rely on the inversion of the auto-correlation sinogram obtained from two-dimensional projections, to form a volumetric estimation of the total auto-correlation of the specimen. The whole process is made possible because the auto-correlation of a signal is always centered in the shift space by definition.

In this proceeding, instead, we describe a new method based on auto-correlation estimation that leads directly to the formation of perfectly aligned and deconvolved reconstructions. We exploit this property to move the reconstruction problem from the direct to the auto-correlation space (or shift space), calculating average auto-correlations of the whole object rather than aligning and averaging the direct observations. Once we do this, we end up with an accurate estimation of the auto-correlation that can be inverted to roll back to the reconstruction

*For the correspondence email to: daniele.ancora@polimi.it

of the sample, without carrying out any alignment procedure. Furthermore, we developed a new algorithmic implementation that simultaneously accomplishes auto-correlation inversion and deblurs via a Bayesian approach. The reconstructions obtained in such a way exhibits higher and isotropic resolution along the spatial directions, with respect the single view dataset, releasing the users from any form of alignment procedure. Since the problem is computationally challenging, we rely on GPUs for the implementation of the algorithm, discussing further developments and novel perspective introduced with the method.

2. MATERIALS AND METHODS

In the present manuscript, we focus on two-dimensional objects, as it would happen if we focus only on a tomographic slice through a sample measured with an LSFM setup. We start from the assumption of having access to two measurements carried out with the same instrument, but at different angular orientations. In Fig. 1A, we present the object that we aim at reconstructing. This is an ideal image of a satellite, commonly used as a testing phantom in image processing pipelines. Let us assume that the ideal object o is measured with an optical imaging setup characterized by its point-spread-function (PSF) h. A generic measurement performed in this case let us measure a blurred estimation of the object:

$$o_{\mu}^{\varphi_i} = o * h + \varepsilon = \int o\left(\boldsymbol{x}\right) h\left(\boldsymbol{\xi} - \boldsymbol{x}\right)\, d\boldsymbol{x}, \tag{1}$$

where $\boldsymbol{x}$ is the coordinate vector in the direct (or object) space and $\boldsymbol{\xi}$ the vector of the auto-correlation (or shift) space. If we assume that the measurement is performed by rotating the sample at a certain angular degree φ_i, and keeping the reference on the object, the effect of the measurement is simply modelled by changing the orientation of the PSF. For our study, we assume h to be a two-dimensional Gaussian function elongated along one direction thus, we choose $\sigma_x = 4.0\, px$ and $\sigma_y = 1.5\, px$ for the first angle $\varphi_0 = 0°$. For a compact notation, we characterize the PSF by its variance along the two spatial direction $\boldsymbol{\sigma} = (\sigma_x, \sigma_y)$. We assume all the signals detected with 16-bit accuracy. In Fig. 1B, we report the result of the measurement after blurring and adding a Poissonian noise term with variance and mean value $\lambda = 2^4$. For the second detection, we assume that the PSF is orthogonal to the previous one, corresponding to a measurement at $\varphi_1 = 90°$. In this case, we model the PSF with a $\boldsymbol{\sigma}_1 = (1.5, 4.0)\, px$ and the result is displayed in Fig. 1C. Here, we add a shift of $(-5, 10)$ pixels in the detection, representing the unknown registration that we would like to avoid estimating. In fact, by a simple average of both detections, we end up with the fuzzy reconstruction displayed in Fig. 1D. In the following, we try to compensate for this by avoiding any registration or alignment task.

2.1 The auto-correlation

The most important quantity that we are interested to compute is the auto-correlation of the object:

$$\chi = o \star o = \int \overline{o\left(\boldsymbol{x}\right)} o\left(\boldsymbol{\xi} + \boldsymbol{x}\right)\, d\boldsymbol{x}. \tag{2}$$

As can be seen by the Fig. 1E, this quantity is always centered by definition and it immediately implies that in the shift-space we do not have to carry out any alignment task. However, we measured a blurred version of the object and, when calculating its auto-correlation, we transport the blurring into the auto-correlation space as:

$$o_{\mu} \star o_{\mu} = (o * h) \star (o * h) = (o \star o) * (h \star h) \tag{3}$$

$$= (o \star o) * \mathcal{H} = \chi * \mathcal{H}, \tag{4}$$

In simple terms, a blurring by h in the direct space is seen as a blurring in the auto-correlation space by $\mathcal{H} = h \star h$. In Fig. 1F,G we report the auto-correlation calculated respectively from the detection at angle $\varphi_0 = 0°$ and $\varphi_1 = 90°$. By calculating the average between these two quantities, we have access to a perfectly aligned auto-correlation estimation (Fig. 1H). We direct our attention to this quantity, which we want to process to roll back to a deconvolved reconstruction in the object space.

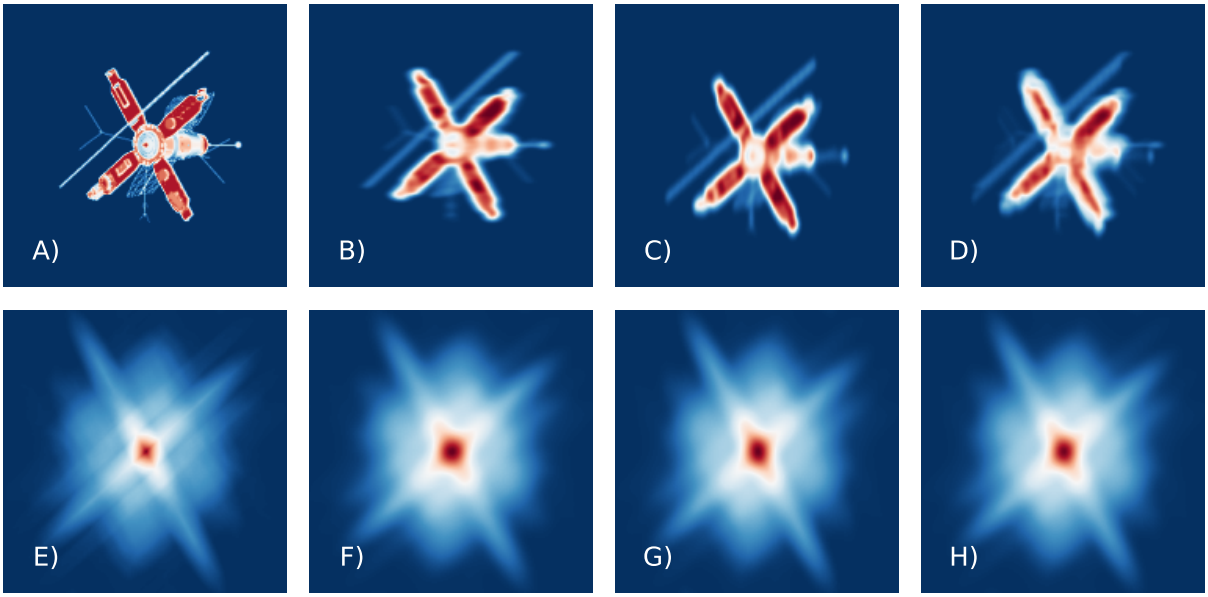

Figure 1. A) Original object $o(\boldsymbol{x})$ that we are interested to reconstruct. B) Blurred detection o^0_μ with $\boldsymbol{\sigma} = (4, 1.5)$. C) Blurred detection o^1_μ using an orthogonal PSF with $\boldsymbol{\sigma} = (1.5, 4)$. The image is shifted with respect the previous detection to simulate a misalignment in the measurement. D) Average of the blurred acquisition $\overline{o}_\mu$. E) Auto-correlation of the original object, χ. F) Auto-correlation, χ^0_μ, of the blurred object as reported in B). G) Auto-correlation, χ^1_μ, of the blurred object as reported in C). H) Average auto-correlations, $\overline{\chi}_\mu$ of the blurred detections.

2.2 Inverting and deblurring the average auto-correlation

So far, we have obtained an estimation of the inherently aligned auto-correlation of the object, starting from two orthogonal and blurred detections. Ideally, the PSF of a perfectly aligned reconstruction of the object is given by the average of the two orthogonal PSF (displayed in Fig. 2A). However, we decided to promote our reconstruction problem in the auto-correlation space in order to avoid alignment issues. In this space, the blurring factor changes into the average $\mathcal{H}$, that can be easily estimated by calculating the auto-correlation of each single PSF in the object space and then averaging. The resulting PSF, $\overline{\mathcal{H}} = h^0 + h^1$ is displayed in Fig. 2B.

Once we have the average auto-correlation $\overline{\chi}_\mu = \chi^0_\mu + \chi^1_\mu$ and the corresponding PSF in the shift-space $\overline{\mathcal{H}}$, we can set up an iterative Bayesian-like algorithm for the reconstruction of the signal. The algorithm is designed by taking inspiration from the Schultz-Snyder method[7] combined with a Richardson-Lucy approach[8,9] for the restoration of a deblurred signal. The protocol is called anchor-update[10] (AU) because it is based on a iterative fix-point multiplication:

$$\mathcal{K}^t_{AU} = o^t \star \overline{\mathcal{H}} \tag{5}$$

$$o^{t+1} = o^t \left[\left(\frac{\overline{\chi}_\mu}{o^t * \mathcal{K}^t_{AU}} \right) * \widetilde{\mathcal{K}}^t_{AU} \right], \tag{6}$$

where o^t is the estimation of the reconstruction after t steps, and $\mathcal{K}^t_{AU}$ is an effective blurring kernel in this representation. For the initial guess $o^{t=0}$ we use a non-null random intensity map. Once we carry out a sufficient number of iterations, the reconstruction is formed and it is possible to analyze.

3. RESULTS AND DISCUSSIONS

The AU protocol solves a problem of the second order with respect to the object o, as in the case of the Schultz-Snyder method. These kind of problems are know to have a slow convergence rate so that we have to set a high

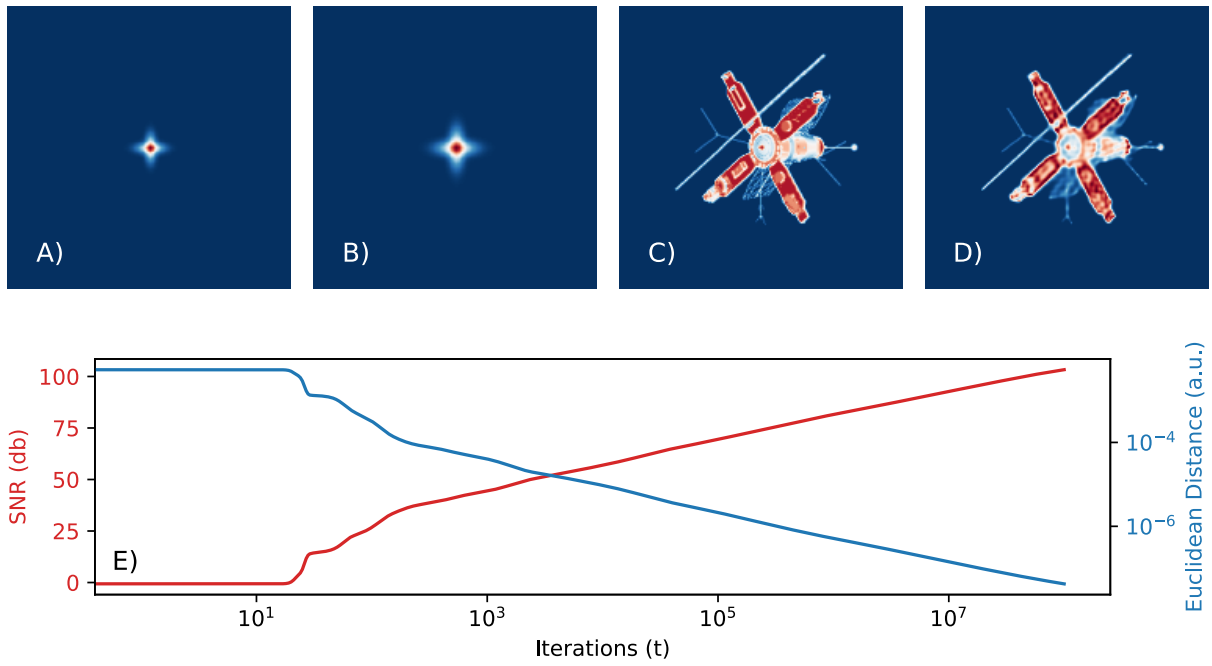

Figure 2. A) Average point-spread-function, $\overline{h}$, of the two orthogonal detections of the object in direct space. This would be exact only in the case that both measurements are perfectly aligned against each other. B) Average point-spread-function, $\overline{\mathcal{H}}$, in the auto-correlation space that we used for our reconstruction method. C) Original object o that we aim at retrieving. D) Object o^t recovered by reconstructing the signal from the auto-correlation average (shown in Fig. 1H) and deconvolved by the PSF in the shift space of panel 1B. E) Distance monitoring for the signal-to-noise ratio (red curve) and the euclidean distance (blue curve) between the blurred auto-correlation average of Fig. 1H and the blurred auto-correlation of the object reconstructed at i-th step.

number of iterations. On the other hand, this is a very robust scheme, implying that the reconstruction quality increases almost constantly as the iteration proceeds. In the present case, we try to push the reconstruction by running a total of 10^8 steps. For completeness, we achieved an improved image quality already after 10^5 steps but, here, we are interested to also study the trend in the reconstruction quality. To monitor the convergence of the reconstruction, we calculate two different measures during the iterations. First, we calculate the SNR between the measured $\overline{\chi}_\mu$ and the estimation auto-correlated and blurred by the PSF in the shift-space $\chi^t = (o^t \star o^t) * \overline{\mathcal{H}}$ as:

$$\mathrm{SNR}\left(\overline{\chi}_\mu \| \chi^t\right) = 20 \log_{10}\left[\frac{\int \overline{\chi}_\mu \, d\boldsymbol{\xi}}{\int \left(\overline{\chi}_\mu - \chi^t\right) \, d\boldsymbol{\xi}}\right]. \tag{7}$$

The second quantity that we monitor is the conventional euclidean distance:

$$d\left(\overline{\chi}_\mu \| \chi^t\right) = \int \left(\overline{\chi}_\mu - \chi^t\right)^2 d\boldsymbol{\xi}. \tag{8}$$

The resulting reconstruction is displayed in Fig. 2D (we report also the original object in Fig. 2C for visual comparison). The quality of the reconstruction is very high, it does not show any alignment issue, and we can appreciate the effect of the deconvolution that sharpened the results simultaneously. The plot underneath, reported in panel 2E, shows the trend for both distances during the iterations. Since the SNR is based on a logarithmic estimation we use a semi-log scale to plot it. Using a log-log scale for the Euclidean distance, let us better compare the curves. Although the quantities are different, their trend is similar but inverted. Of course, we are looking for the signal that maximizes the SNR, whereas we also look for the one that minimize the Eu-

clidean distance. Both measures continue to be optimized as the iterations proceed, due to the robust behaviour of the algorithm. We conclude that monitoring just one of these two is sufficient for having an indication of the reconstruction quality achieved. These are promising results in the field of registration-free tomography, since we are forming a reconstruction free of any misalignment issues given any arbitrary number of independent measurements. We are currently investigating the application of the present method with experimental measurements in light-sheet microscopy,[11] and we are exploring new implementations of the algorithm to force smoothness in the reconstruction behaviour.

ACKNOWLEDGMENTS

The research has received support from the European Union's Horizon 2020 research and innovation programme under the Marie Sklodowska-Curie project (H2020-MSCA-IF-2017, project acronym: HI-PHRET, G.A. 799230) and under H2020 Laserlab Europe V (G.A. 871124). The authors thank Dr. Gianmaria Calisesi and Elena Corbetta for inspiring discussions.

REFERENCES

[1] Power, R. M. and Huisken, J., "A guide to light-sheet fluorescence microscopy for multiscale imaging," *Nature methods* **14**(4), 360–373 (2017).

[2] Krzic, U., Gunther, S., Saunders, T. E., Streichan, S. J., and Hufnagel, L., "Multiview light-sheet microscope for rapid in toto imaging," *Nature methods* **9**(7), 730–733 (2012).

[3] Preibisch, S., Amat, F., Stamataki, E., Sarov, M., Singer, R. H., Myers, E., and Tomancak, P., "Efficient bayesian-based multiview deconvolution," *Nature methods* **11**(6), 645 (2014).

[4] Rieckher, M., Psycharakis, S. E., Ancora, D., Liapis, E., Zacharopoulos, A., Ripoll, J., Tavernarakis, N., and Zacharakis, G., "Demonstrating improved multiple transport-mean-free-path imaging capabilities of light sheet microscopy in the quantification of fluorescence dynamics," *Biotechnology journal* **13**(1), 1700419 (2018).

[5] Ancora, D., Di Battista, D., Giasafaki, G., Psycharakis, S. E., Liapis, E., Ripoll, J., and Zacharakis, G., "Phase-retrieved tomography enables mesoscopic imaging of opaque tumor spheroids," *Scientific reports* **7**(1), 11854 (2017).

[6] Ancora, D., Di Battista, D., Vidal, A. M., Avtzi, S., Zacharakis, G., and Bassi, A., "Hidden phase-retrieved fluorescence tomography," *Optics Letters* **45**(8), 2191–2194 (2020).

[7] Schulz, T. J. and Snyder, D. L., "Image recovery from correlations," *JOSA A* **9**(8), 1266–1272 (1992).

[8] Lucy, L. B., "An iterative technique for the rectification of observed distributions," *The astronomical journal* **79**, 745 (1974).

[9] Richardson, W. H., "Bayesian-based iterative method of image restoration," *JoSA* **62**(1), 55–59 (1972).

[10] Ancora, D. and Bassi, A., "Deconvolved image restoration from auto-correlations," *IEEE Transactions on Image Processing* **30**, 1332–1341 (2020).

[11] Ancora, D., Valentini, G., Pifferi, A., and Andrea, B., "Beyond multi-view deconvolution for inherently-aligned fluorescence tomography," *arXiv preprint arXiv:2102.08177* (2021).